

Waveguide Microwave Imaging: Solids Volume Fraction of Particulate Materials

Alexander V. Brovko¹, Ethan K. Murphy^{2,3}, and Vadim V. Yakovlev²

¹Department of Applied Information Technologies
Yury Gagarin State Technical University of Saratov (SSTU), Saratov 410054, Russia
brovkoav@gmail.com

²Department of Mathematical Sciences
Worcester Polytechnic Institute, Worcester, MA 01609, USA
vadim@wpi.edu

³Thayer School of Engineering
Dartmouth College, Hanover, NH 03755, USA
ethan.k.murphy@dartmouth.edu

Abstract — An original modeling-based microwave imaging technique for determining the volume fraction of solid material in dielectric powders is described. The desired characteristic is determined by analyzing S -parameter measurements in a waveguide containing the sample with the help of an artificial neural network trained by data from 3D FDTD simulation. The powder sample is represented by a mixture of air and millimeter-scale particles reproduced in the FDTD model. Computational tests with 20 to 40 mm cubic samples of SiC and ZrO₂ powders in WR340 show that the solids volume fraction is determined with less than 5% error.

Index Terms — Artificial neural network, FDTD modeling, microwave imaging, particulate materials, solids volume fraction.

I. INTRODUCTION

High-temperature microwave processing methods, including sintering, are known to be promising technologies that, when carried out in properly designed systems, could facilitate energy savings and high quality processing of powders and particulate materials [1-4]. There is a growing effort to develop corresponding multiphysics models and computational tools capable of assisting engineers in designing systems for efficient high-temperature microwave processing (see, e.g., [5-9]). Characterization of material properties is an integral part of the modeling process, but reliable experimental data on electromagnetic and thermal parameters of the processed material are not always available.

Thermal conductivity is a critically important input parameter in the computation of microwave-induced temperature fields. For many powders, it can be relatively

accurately estimated using advanced physical models for thermal conductivity of porous materials [10,11]. However, this approach requires the solids volume fraction ϕ (or porosity $\psi = 1 - \phi$) of the powder to be known. For many materials the data provided by the manufacturers or in handbooks is available in only a certain range, so the resulting value of thermal conductivity becomes necessarily uncertain [12]. This, in turn, may impact the results of computer simulation.

Effective complex permittivity ϵ_{eff} is another critical input parameter of the related multiphysics models. All (classical and contemporary) mixing formulas which can be used for determining ϵ_{eff} of the powder material (interpreted as a mixture of air and a solid component) require ϕ to be a known parameter [13].

Data on ϕ is also important to the accurate design and valid modeling of behavior of particulate materials in fluidized beds, solid fuel combustion, and other industrial processes. While a variety of measurement techniques (including non-invasive microwave and optical sensing methods) have been reported [14-18], experimental determination of the concentration of solid in these applications may be technically difficult, expensive and not always practically possible.

In this paper, we describe an original modeling-based microwave imaging technique for determining the solids volume fraction of dielectric particulate materials. The proposed approach further develops the authors' earlier artificial neural network (ANN) inversion technique for finding the position and size of an object inside a dielectric sample in a waveguide system [19,20]. The ANN is trained with multiple S -parameter data from full-wave numerical simulations; the network determines ϕ when it is given the data on a corresponding single

measurement. In the model, a sample of micro- or nano-powder is represented by a collection of inclusions (comparable in their dimensions with the size of the unit of spatial discretization) enclosed in the sample's volume. Legitimacy of such a representation is supported by computational tests showing an insensitivity of frequency characteristics of the S -parameters to the particle size in different scenarios with the same ϕ . We find that both solid-in-air and air-in-solid material models are operational with the inclusions of both rectangular and cylindrical shapes, but the model with air parallelepipeds in solid appears to be computationally most efficient. Functionality of the proposed technique is demonstrated with silicon carbide (SiC) and zirconium dioxide (ZrO₂) (zirconia) powders in a rectangular waveguide; the solids volume fraction of the powders with $\phi = 60$ -80% is reconstructed with less than 5% error.

II. TECHNIQUE AND MATERIALS

Our approach to determining the solids volume fraction of powders and particulate materials is based on simple measurement of S -parameters of a waveguide containing a tested sample and an ANN inversion procedure, backed by data on the reflection coefficient S_{11} and the transmission coefficient S_{21} in a finite-difference time-domain (FDTD) simulation of this system. We consider complex reflection and transmission coefficients in a two-port waveguide structure shown in Fig. 1; for the sake of computational convenience, the tested powder material is considered in this paper to be of rectangular shape of A , B , and C mm in the directions of the x -, y -, and z -axes, respectively. In principle, the technique remains the same for the samples of any shape, and the measurement system remains the same for the samples of different shapes and sizes.

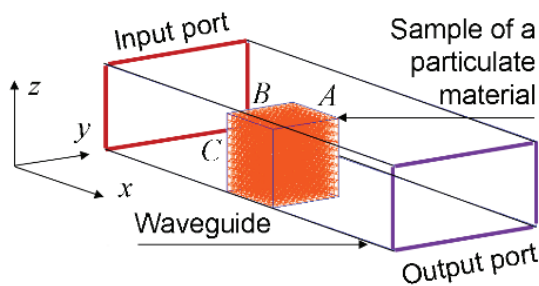


Fig. 1. Microwave system with the tested sample; output port is supposed to be a perfect load.

We introduce the characteristic of the solids volume fraction ϕ assuming that the sample consists of two media, air and solid, and they are arranged as in one of the lattices in Fig. 2: multiple solid inclusions (of rectangular or cylindrical shape) in air, or multiple air inclusions (of rectangular or cylindrical shape) in solid. While typical powders to be sintered consist of micro- or

nanometer particles, the sizes of the inclusions in our technique are comparable with cells in an applicable practical FDTD mesh; thus, for the microwave frequency range, they are of millimeter-scale size. Two examples of a volumetric structure of the tested sample (taken for convare) shown in Fig. 3.

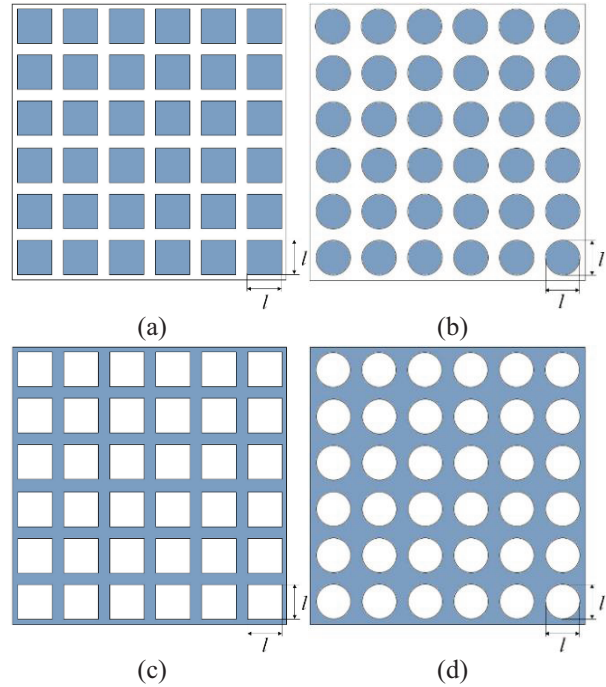


Fig. 2. Solid-in-air (a), (b) and air-in-solid (c), (d) models of a particular material – cubic/rectangular (a), (c) and cylindrical (b), (d) inclusions.

The adequacy of such a representation is suggested by the key principle of microwave imaging: the observed electric field responses to the effective complex permittivity of a dielectric mixture that depends on the volume fraction of the inclusions rather than on their individual dimensions. Furthermore, following the classical mixing approach [13], in this paper, we work with the samples in which the inclusions are assumed to be of sizes randomly distributed within certain ranges and randomly positioned within their immediate neighborhoods. The solids volume fraction ϕ is calculated as the ratio:

$$\phi = V_i/V_s,$$

where V_s is the volume of the sample (in our case, $V_s = ABC$) and V_i is the total volume occupied by the inclusions and calculated as:

$$V_i = \begin{cases} \sum_{j=1}^N a_j b_j c_j, & \text{for rectangular inclusions,} \\ \sum_{j=1}^N \pi \left(\frac{d_j}{2}\right)^2 h_j, & \text{for cylindrical inclusions,} \end{cases}$$

where a_j , b_j , c_j , d_j , and h_j are the dimensions of N rectangular or cylindrical inclusions, as shown in Fig. 3.

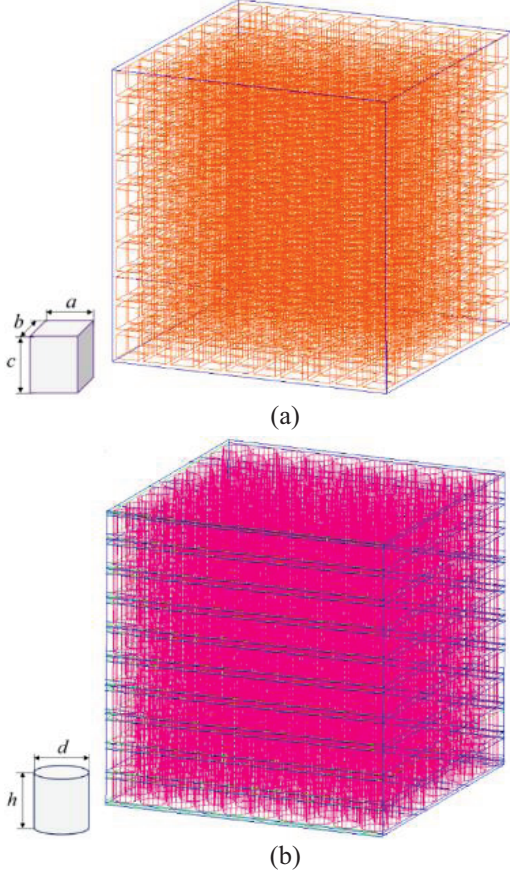


Fig. 3. 3D views of the tested samples with rectangular boxes (a) and cylinders (b) homogeneously embedded as inclusions in an isotropic environment of cubic shape.

We use an ANN with global cubic radial basis functions (RBF) for single hidden layer neurons [21,22] as an inversion mechanism for determining ϕ of the powder in the sample. The network architecture is shown in Fig. 4. The ANN inputs, \mathbf{X} , are the real and imaginary parts of the S -parameters at P points in the considered frequency range ($4P$ input nodes); the output of the ANN is the predicted value of solids volume fraction ϕ^* . The hidden layer of neurons consist of N_C nodes, which have form:

$$g_i(\mathbf{X}) = \|\mathbf{X} - \mathbf{C}_i\|^3,$$

where \mathbf{C}_i are the centers of the RBFs and $i = 1, \dots, N_C$. The S -parameters of the waveguide system partially filled with the sample (Fig. 1) are computed with the FDTD model and used for ANN training. For each simulation, a distribution of inclusions in the sample is generated assuming the particles to be of sizes randomly distributed from l_1 to l_2 mm. It is also assumed that $a \ll A$, $b \ll B$, $c \ll C$, and that a, b, c are much less than the wavelength in the waveguide.

The output of the ANN is a linear combination of outputs from each RBF. The trained network finds the

weights, i.e., coefficients of each RBF, such that the linear system is best fit in a least squares sense. That is, given N_T training samples, we have N_T input-output pairs (\mathbf{X}_j, ϕ_j) , so, to train the network, we find a solution to the linear system:

$$\mathbf{G}(\mathbf{X})\mathbf{w} = \begin{bmatrix} g_1(\mathbf{X}_1) & g_2(\mathbf{X}_1) & \dots & g_{N_C}(\mathbf{X}_1) \\ g_1(\mathbf{X}_2) & g_2(\mathbf{X}_2) & \dots & g_{N_C}(\mathbf{X}_2) \\ \vdots & \vdots & \ddots & \vdots \\ g_1(\mathbf{X}_{N_T}) & g_2(\mathbf{X}_{N_T}) & \dots & g_{N_C}(\mathbf{X}_{N_T}) \end{bmatrix} \begin{bmatrix} w_1 \\ w_2 \\ \vdots \\ w_{N_C} \end{bmatrix} = \begin{bmatrix} \phi_1 \\ \phi_2 \\ \vdots \\ \phi_{N_T} \end{bmatrix} = \boldsymbol{\phi},$$

with the weight vector \mathbf{w} . We employ a zero training error regime for selection of centers, i.e., the training set is the set of centers chosen [23]. This means that $N_C = N_T$ and $\mathbf{G}(\mathbf{X})$ is a $N_T \times N_T$ matrix. The trained network in Fig. 4 can therefore be described by the formula:

$$\mathbf{G}(\mathbf{X})\mathbf{w}^* = \boldsymbol{\phi}^*,$$

where \mathbf{w}^* is the best fitting weights and $\boldsymbol{\phi}^*$ is the ANN's approximation to $\boldsymbol{\phi}$. The linear system is solved using singular value decomposition.

After sufficient training, the ANN is able to reconstruct the solids volume fraction of the tested material from S -parameters obtained by a physical measurement. While in general this technique of numerical inversion is similar to our earlier ANN methodology [19,20], here it results not in reconstruction of parameters of each individual inclusion, but in the characteristic of their group with possible random deviations in their positions and sizes.

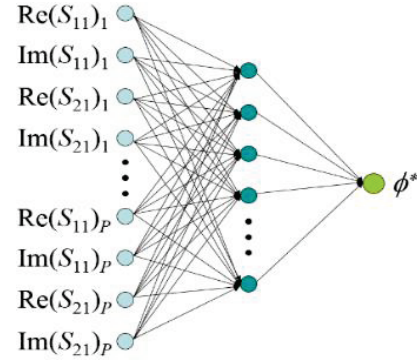


Fig. 4. The ANN structure with one hidden layer.

III. RESULTS

The proposed technique was tested with three cubic samples ($A = B = C = 40, 30$, and 20 mm) of SiC and ZrO_2 powder in a section of WR340 waveguide of 250 mm length. For the considered range around the frequency of microwave sintering (2.45 GHz), we chose, in order to keep the required CPU time reasonable, the minimum cell size of the FDTD model to be 0.5 mm; therefore, the size distribution of the inclusions was chosen between $l_1 = 2$ mm and $l_2 = 8$ mm. The dielectric constant ϵ' and electric conductivity σ of the bulk materials were taken

to be $\epsilon' = 10.4$ and $\sigma = 0.1225$ S/m for SiC [1] and $\epsilon' = 6.69$ and $\sigma = 0.0258$ S/m for ZrO₂ [24].

The underlying computation of S -parameters was performed with the 3D conformal FDTD simulator QuickWave 2014 [25]. In the process of ANN training, we applied a coarse mesh with cell size 1 mm inside the sample and 5 mm outside the sample; the number of cells was 138,000, and steady state was reached after about 10,000 iterations. One single simulation took about 1.5 minutes on a PC with an AMD Athlon 6000+ 3 GHz processor. When computing S -parameters for different sizes of inclusions, we applied a finer mesh with cell size 0.5 mm inside the sample and 5 mm outside the sample; in this case, the number of cells in the model was near 1 million, and steady state was reached after about 25,000 iterations. A single run on the aforementioned PC took about 30 minutes.

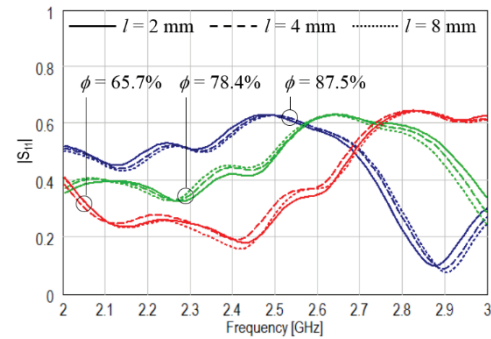
All material models presented in Fig. 2 were tested, and while all four were found operational, the FDTD model with rectangular air-in-solid inclusions turned out to be most efficient (as required minimum computational resources) as well as stable and controllable: the lattice in Fig. 2 (c) can be kept in quite wide ranges of l and ϕ .

A series of frequency-dependent characteristics of $|S_{11}|$ typical for the air-in-solid rectangular inclusions in the cubic sample are shown in Fig. 5. It can be seen that the curves corresponding to different particle sizes, but the same solids volume fraction, are very close to each other, whereas the curves corresponding to different ϕ are fairly distinct. ($|S_{21}|$ curves are not presented here, but their behavior is very similar.) The computations suggest that we can expand the results obtained for the samples with large (millimeter-scale) inclusions to samples of powders containing micro- and/or nanometer-scale particles without reproducing their actual sizes with the nano-scale cells of the FDTD model.

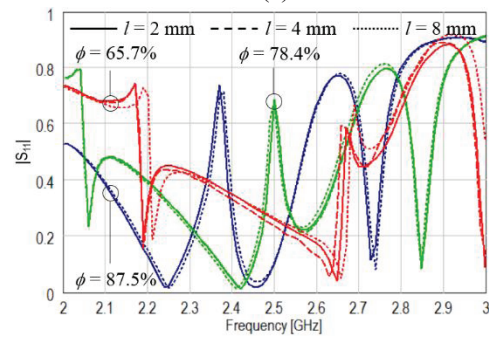
The diagrams in Figs. 6-7 characterize the quality of learning of the ANN with $P = 21$ (i.e., with 20 equal intervals in the 2 to 3 GHz frequency range) for random-size particle distributions and different shapes of the inclusions. For both powders and both air-in-solid and solid-in-air material models, the ANN is trained with 800 distributions of particles of the material in air. It is seen that for cubic samples larger than 20 mm in size, reconstructed values of ϕ appear to be very close to the testing values.

Table 1 shows the reconstructed solids volume fractions of six samples in comparison with their actual values. For powders of lower density ($\phi < 0.75$), the reconstruction error does not exceed 1.5%. When the sample appears to be closer to a solid ($\phi \sim 0.8$), the reconstruction is less accurate, but the errors are still less than 5%. The accuracy is worse in the case of small samples with low-density powders. Since in these examples, the experimental data for S -parameters are

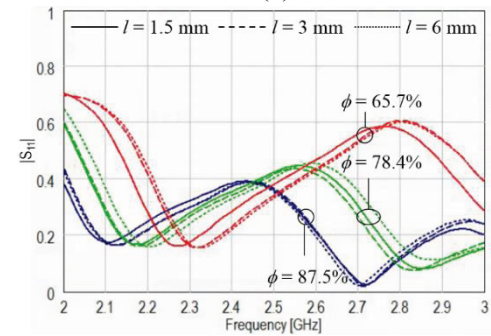
simulated using a computer model, we expect that a practical implementation of this technique might suffer somewhat lower accuracy. However, the reconstructed solids volume fraction is still anticipated to be sufficiently accurate for subsequent use in physical models for thermal conductivity, especially in the absence of experimental data, and in other applications.



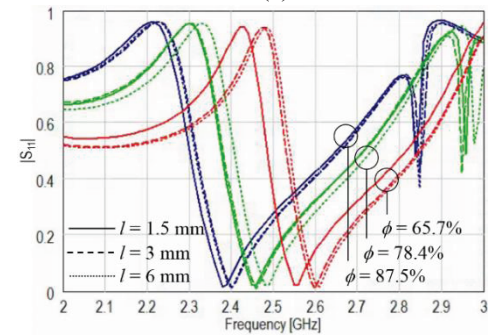
(a)



(b)



(c)



(d)

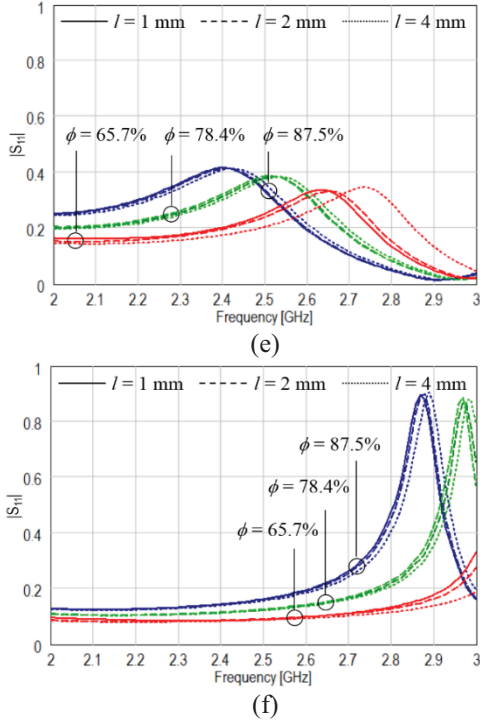


Fig. 5. Frequency characteristics of $|S_{11}|$ for different particle size l and solids volume fraction ϕ in the lattice Fig. 2 (c) for cubic samples $A = B = C = 20$ mm (a, b), 30 mm (c, d), and 40 mm (e, f) of SiC (a), (c) (e) and ZrO₂ (b), (d), (f).

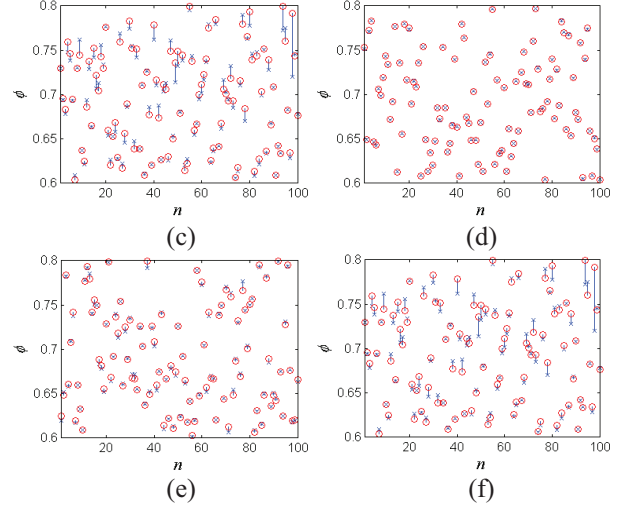
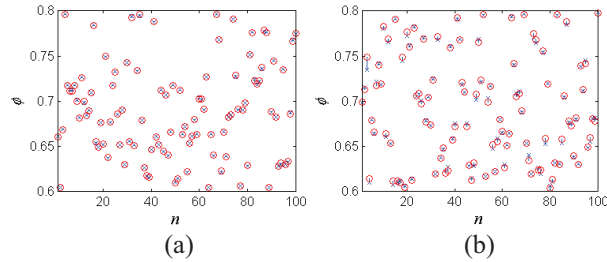


Fig. 6. ANN performance for the system with a solid-in-air (Fig. 2 (a)) cubic sample $A = B = C = 20$ mm (a), (d), 30 mm (b), (e), and 40 mm (c), (f) of SiC power (a)-(c) and ZrO₂ powder (d)-(f) represented by rectangular inclusions for $n = 100$ testing points; \times : testing points; o : network responses.

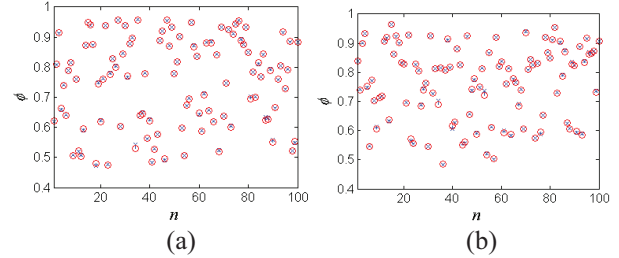


Fig. 7. ANN performance for the system with an air-in-solid (Fig. 2 (c)) cubic sample $A = B = C = 30$ mm of SiC power (a) and ZrO₂ powder (b) represented by cylindrical inclusions for $n = 100$ testing points; \times : testing points; o : network responses.

Table 1: Solids fractions of the powders reconstructed by the trained ANN

Powder	Sample: 40×40×40 mm			30×30×30 mm		20×20×20 mm	
	Actual ϕ	Reconstructed ϕ	Relative Error (%)	Reconstructed ϕ	Relative Error (%)	Reconstructed ϕ	Relative Error (%)
SiC	0.60	0.601	0.1	0.603	0.5	0.644	7.3
	0.65	0.643	1.1	0.644	0.9	0.649	0.2
	0.70	0.690	1.4	0.704	0.6	0.701	0.1
	0.75	0.746	0.5	0.747	0.4	0.748	0.3
	0.80	0.766	4.3	0.792	1.0	0.801	0.1
ZrO ₂	0.60	0.597	0.5	0.601	0.2	0.463	22.8
	0.65	0.643	1.1	0.641	1.4	0.649	0.2
	0.70	0.690	1.4	0.707	1.0	0.701	0.1
	0.75	0.751	0.1	0.748	0.3	0.749	0.1
	0.80	0.777	2.9	0.790	1.3	0.801	0.1

IV. CONCLUSION

A new modeling-based technique for determining the solids volume fraction of particulate materials by the means of waveguide microwave imaging has been outlined. The required characteristic is extracted from S -parameters of a waveguide system containing the tested sample and is independent on the size of millimeter-scale inclusions representing micro- and nano-particles of the powder. It has been shown that, when backed by FDTD data in the 2 to 3 GHz frequency range, the ANN with global cubic RBF determines ϕ with a sufficiently high resolution. Functionality of the technique has been illustrated in computational experiments with silicon carbide and zirconia powders. It was shown that with both materials excellent accuracy (less than 5% error) was achieved. It should be noted that this level of quality of reconstruction is reached with the use of minimal computational resources.

In further developments, with an appropriate alteration of the ANN structure, the proposed technique can be transformed for determining the effective complex permittivity of particulate materials.

REFERENCES

- [1] D. E. Clark and W. H. Sutton, "Microwave processing of materials," *Annual Review of Material Science*, vol. 26, pp. 299-331, 1996.
- [2] Y. V. Bykov, K. I. Rybakov, and V. E. Semenov, "High-temperature microwave processing of materials," *J. Phys. D: Appl. Phys.*, vol. 34, pp. R55-75, 2001.
- [3] M. Oghbaei and O. Mirzaee, "Microwave versus conventional sintering: a review of fundamentals, advantages and applications," *J. Alloys and Compounds*, vol. 494, pp. 175-189, 2010.
- [4] D. Agrawal, "Microwave sintering of ceramics, composites and metallic materials, and melting of glasses," *Trans. Indian Ceramic Soc.*, vol. 65, pp. 129-144, 2006.
- [5] Y. Duan, D. C. Sorescu, and J. K. Johnson, "Finite element approach to microwave sintering of oxide materials," *Proc. COMSOL Users Conference*, Boston, 2006.
- [6] D. Bouvard, S. Charmond, and C. P. Carry, "Multiphysics simulation of microwave sintering in monomode cavity," *Ceram. Trans.*, vol. 209, pp. 173-180, 2010.
- [7] S. A. Bogachev, D. Bouvard, E. M. Kiley, and V. V. Yakovlev, "A macroscopic iterative routine for modeling electromagnetic, thermal, and mechanical phenomena in microwave sintering," in *Microwave and RF Power Applications*, J. Tao, Ed., Cépaduès Éditions, pp. 372-375, 2011.
- [8] K. I. Rybakov, E. A. Olevsky, and E. V. Krikun, "Microwave sintering: fundamentals and modeling," *J. Am. Ceram. Soc.*, vol. 96, pp. 1003-1020, 2013.
- [9] E. M. Moon, C. Yang, and V. V. Yakovlev, "Microwave-induced temperature fields in cylindrical samples of graphite powder - experimental and modeling studies," *Intern. J. Heat & Mass Transfer*, vol. 87, pp. 359-368, 2015.
- [10] P. Cheng and C-T. Hsu, "The effective stagnant thermal conductivity of porous media with periodic structures," *J. Porous Media*, vol. 2, pp. 19-38, 1999.
- [11] M. Kandula, "On the effective thermal conductivity of porous packed beds with uniform spherical particles," *J. Porous Media*, vol. 14, pp. 919-926, 2011.
- [12] E. M. Moon, C. Yang, M. Patel, H. He, and V. V. Yakovlev, "Microwave-induced temperature fields in graphite powder heated in a waveguide reactor," *IEEE MTT-S Intern. Microwave Symp. Dig.*, Tampa, FL, 978-1-4799-3869-8/14, June 2014.
- [13] A. Sihvola, *Electromagnetic Mixing Formulas and Applications*, IEE, London, 1999.
- [14] H. Johnsson and F. Johnsson, "Measurements of local solids volume-fraction in fluidized bed boilers," *Powder Technology*, vol. 115, pp. 13-26, 2001.
- [15] J. M. Link, W. Godlieb, P. Tripp, N. G. Deen, S. Heinrich, J. A. M. Kuipers, M. Schönherr, and M. Peglow, "Comparison of fibre optical measurements and discrete element simulations for the study of granulation in a spout fluidized bed," *Powder Technol.*, vol. 189, pp. 202-217, 2009.
- [16] Y. Liu, Z. Huang, H. Ji, and H. Li, "Solid volume fraction measurement of gas-solid two-phase flow based on terahertz time-domain spectroscopy technique: a preliminary study and static experimental results," *IEEE Trans. Instrum. Meas.*, vol. 58, pp. 1585-1592, 2009.
- [17] J-P. Laviolette, G. S. Patience, and J. Chaouki, "Fibre-optic probe for the simultaneous measurement of gaseous species composition and solids volume fraction," *Proc. 13th Intern. Conf. on Fluidization - New Paradigm in Fluidization Engineering*, Montreal, 2010.
- [18] G. Xu, C. Liang, X. Chen, D. Liu, P. Xu, L. Shen, and C. Zhao, "Investigation on dynamic calibration for an optical-fiber solids concentration probe in gas-solid two-phase flows," *Sensors*, vol. 13, pp. 9201-9222, 2013.
- [19] A. V. Brovko, E. K. Murphy, M. Rother, H. P. Schuchmann, and V. V. Yakovlev, "Waveguide microwave imaging: spherical inclusion in a dielectric sample," *IEEE Microwave and Wireless Comp. Lett.*, vol. 18, pp. 647-649, 2008.
- [20] A. V. Brovko, E. K. Murphy, and V. V. Yakovlev, "A modeling-based technique for nondestructive evaluation of metal powders undergoing microwave sintering," *IEEE MTT-S Intern. Microwave Symp. Dig.*, Anaheim, CA, pp. 1428-1431, May 2010.

- [21] E. K. Murphy and V. V. Yakovlev, "RBF network optimization of complex microwave systems represented by small FDTD modeling data sets," *IEEE Trans. Microwave Theory Tech.*, vol. 54, pp. 3069-3083, 2006.
- [22] A. V. Brovko, E. K. Murphy, and V. V. Yakovlev, "Waveguide microwave imaging: neural network reconstruction of functional 2-D permittivity profiles," *IEEE Trans. Microwave Theory Tech.*, vol. 57, pp. 406-414, 2009.
- [23] M. Kirby, *Geometric Data Analysis*, Wiley, New York, 2001.
- [24] V. V. Yakovlev, S. M. Allan, M. L. Fall, and H. S. Shulman, "Computational study of thermal runaway in microwave processing of zirconia," in *Microwave and RF Power Applications*, J. Tao, Ed., Cépaduès Éditions, pp. 303-306, 2011.
- [25] QuickWave 2014™, QWED Sp. z o. o., <http://www.qwed.com.pl/>.



Alexander V. Brovko received the M.Sc. and Ph.D. degrees in Radio Physics and Electronics from Saratov State University, Saratov, Russia, in 1996 and 1999, respectively. From 1999 to 2005, he was an Assistant Professor and Associate Professor with Saratov

State University. Since 2005, he has been with the Department of Applied Information Technologies, Saratov State Technical University (SSTU), where he is currently Associate Professor. From 2010 to 2012, he served as the Vice-Dean of Research at the Faculty of Applied Information Technologies.

Starting 2000, Brovko held a number of short-term Visiting Research positions in Chalmers University of Technology, Swiss Federal Laboratories for Materials Science and Technology, Democritus University of Thrace, and Karlsruhe Institute of Technology. He has authored over 50 papers in referred journals and conference proceedings. His research interests include computational electromagnetics, finite element and FDTD methods, optimization techniques, inverse electromagnetic problems, and optical devices.



Ethan K. Murphy received the M.S. degree in Industrial Mathematics from Worcester Polytechnic Institute (WPI), Worcester, MA in 2003 and the Ph.D. degree in Mathematics from Colorado State University, Fort Collins, CO in 2007. He then held

research and teaching positions at WPI, Rensselaer

Polytechnic Institute, and Applied Mathematics, Inc. Currently he is a Research Associate at Dartmouth's Thayer School of Engineering studying Medical Imaging and in particular Electrical Impedance Tomography. His research interests include inverse problems, microwave optimization, microwave imaging, and computational mathematics. He has authored more than 40 papers in referred journals and conference proceedings. Murphy is a Member of SIAM and Pi Mu Epsilon.



Vadim V. Yakovlev received his Ph.D. degree in Radio Physics from Institute of Radio Engineering and Electronics (IRE) of the Russian Academy of Sciences (RAS), Moscow, Russia in 1991. From 1984 to 1996, he held junior to senior research positions with the IRE RAS and in 1993 worked as Visiting Researcher at Electricité de France (Centre "Les Renardières").

In 1996, he joined the Department of Mathematical Sciences, Worcester Polytechnic Institute, Worcester, MA and currently holds there a position of Research Associate Professor. Yakovlev is a Head of the Industrial Microwave Modeling Group which he established in 1999 as a division of the WPI's Center for Industrial Mathematics and Statistics. Yakovlev's research interests in computational electromagnetics include neural-network-based optimization, microwave imaging, multiphysics modeling, microwave power engineering, and broadband/multiband antennas. He is an author of more than 150 papers in referred journals and conference proceedings. Yakovlev is a Senior Member of the IEEE and a Member of the IEEE MTT-S IMS TPRC. He is a Member of the Board of Governors of International Microwave Power Institute (IMPI), a Member of Association for Microwave Power in Europe for Research and Education (AMPERE) and a Member of the Massachusetts Institute of Technology (MIT) Electromagnetics Academy. He serves as a Reviewer for several journals and as a Member of program committees of several conferences.